Rhythmic Fluctuations in Evidence Accumulation during Decision Making in the Human Brain

Valentin Wyart, Vincent de Gardelle, Jacqueline Scholl, and Christopher Summerfield

Pages: 15; Figures: 7

Contents:

Supplemental Results

Here we describe seven additional control analyses that we performed to provide further support to the main findings described in the article. Each control analysis is linked to one of the main figures (in ascending order), and is accompanied by a supplemental figure summarising its results.

Orthogonal contributions of successive elements to choice

We performed an additional behavioural analysis to test whether successive decision updates contributed independently to the final choice (Figure S1). To do so, we performed a logistic regression analysis where we entered the category of each element k (+1: cardinal or −1: diagonal) and tested whether not only the magnitude of the decision update DU_k, but also the magnitudes of previous and next decision updates DU_{k-1} and DU_{k+1}, influenced the contribution of element k to choice. We found that this was not the case: for any given element k, only DU_k influenced its contribution to choice as measured by its parameter estimate (t-test against zero, $t_{14} = 13.7$, $p < 0.001$). Critically, DU_{k-1} and DU_{k+1} did not influence the contribution of element k to choice (k−1: $t_{14} = 1.3$, $p > 0.2$; k+1: $t_{14} = 1.4$, $p = 0.2$).

This additional finding is important, because it shows that the refractory pattern of decision weighting observed across successive elements cannot be due to the particular sequence of decision updates we provided to the participants, but only to the ongoing phase of endogenous cortical oscillations measured using EEG.

Overlapping neural encoding of successive perceptual and decision updates

We engineered our sequences so that successive perceptual/decision updates were uncorrelated (Figure S1). This feature not only ensured that we could regress individual decision weights with the highest statistical power, but also that we could regress the distinct contributions of successive decision updates against single-trial EEG signals without contamination between temporally adjacent elements.

Nevertheless, to confirm the fact the encoding time courses at $t > t_k + 250$ ms were not contaminated by the overlapping encoding of element k+1 in single-trial EEG signals, we conducted an additional regression analysis where we regressed single-trial EEG signals not only against the perceptual/decision update corresponding to element k, but simultaneously against the perceptual/decision updates corresponding to previous (k−1) and next elements (k+1). If the encoding time courses shown on Figure 2 were contaminated by temporally adjacent elements, then this multiple regression analysis should reveal different temporal profiles. However, we found that this was not the case (Figure S2): the encoding of successive perceptual/decision updates followed the same temporal profile, shifted by 250 ms as expected by our 4 Hz presentation rate. This additional control analysis confirms that we could successfully regress the overlapping neural encoding of successive updates in single-trial EEG signals.

Overlapping neural decoding of successive decision weights

As described above, we found that successive elements contributed independently to the eventual choice – in other words, that the contribution of element k to choice depended solely on decision update DU_k, not on previous and next decision updates DU_{k-1} and DU_{k+1}. This observation rules

out the possibility that the refractory pattern of decision weighting we observed across successive elements (Figure 3C) could be explained by an exogenous influence of DU_{k-1} or DU_{k+1} on the decision weight w_k rather than by an endogenous cortical rhythm.

Nevertheless, to confirm that the refractory pattern of decision weighting was due to ongoing fluctuations in EEG signals, we performed an additional control analysis where we estimated simultaneously the decoding time courses of successive decision weights assigned to previous (k−1), current (k) and next (k+1) elements in the final choice (Figure S3). To do so, we used a multiple psycho-physiological interaction for which the decision information corresponding to previous, current and next elements was partialled out. The three successive decoding time courses show identical patterns shifted by 250 ms, confirming that the decoding results reported later than 250 ms following element k are not due to spurious interactions between choice and the decision information provided by the next element.

Besides, in accordance with the pattern observed in Figure 3, Figure S3 depicts the relationship between encoding residuals around 500 ms following element k and the decision weights assigned to previous (k−1), current (k) and next (k+1) elements in the final choice. Figure S3 shows unambiguously that, at the same point in time, encoding residuals correlate positively with the decision weight assigned to the element k, and negatively with the decision weights assigned to element k−1 and k+1. Importantly, because encoding residuals reflect trial-to-trial EEG variability unexplained by the successive decision updates, variability in encoding residuals was fully uncorrelated (across trials) with variability in decision updates for every participant. Figure S3 also illustrates this pattern of results by showing the spatial distributions of neural encoding and decoding for successive decision updates and decision weights at the same point in time – at 500 ms following element k, obtained using the same multivariate regression approach.

Oscillatory properties of slow fluctuations in neural encoding

We performed several control analyses to rule out the possibility that the modulation of neural encoding and decision weighting by slow EEG fluctuations could be due to a single-sided transient in broadband EEG signals, rather than to a genuine rhythmic process oscillating at about 2 Hz.

To do so, we tested whether the first (negative) encoding component of decision update DU_k (Figure 2), peaking around 300 ms following element k, also depended on delta phase. We found that this was the case (Figure S4), and that the preferred phase for this first encoding component corresponded to the trough of the delta cycle – in other words, the anti-phase of the preferred phase for the second (positive) encoding component of decision update DU_k peaking at 500 ms following element k. Because the two encoding components are separated in time by approximately 250 ms, this opposite phase relationship is fully predicted by a preferred delta oscillation reaching its trough at 250 ms, and then its peak at 500 ms following element k.

Furthermore, although both the P1-like encoding component of PU_k (at 120 ms following element k) and the P3-like encoding component of DU_k (at 500 ms following element k) were positive-going (Figure 2), their preferred delta phases were very different (Figure 4). Again, the phase relationship observed between these two encoding components is consistent with a preferred delta oscillation reaching its trough at 250 ms and its peak at 500 ms following element k. These findings thus argue in favour of a genuine rhythmic process modulating the neural encoding of successive perceptual/decision updates at approximately 2 Hz. Interestingly, the preferred delta oscillation

predicted with respect to decision weight w_k matches the preferred phase with respect to the neural encoding of both perceptual update PU_k and decision update DU_k (Figure S4).

Oscillatory properties of slow fluctuations in decision weighting

We also conducted additional control analyses to further show that the modulation of decision weighting followed the phase of a genuine rhythm reflected in the phase of slow EEG oscillations, not single-sided transients in broadband EEG signals as the ones corresponding to the steady-state response depicted on Figure S5.

First, we observed that the latency t* at which delta phase, estimated analytically using the Hilbert transform applied to band-pass-filtered EEG signals between 1 and 4 Hz, predicted maximally the decision weight w_k followed the onset of element k by 420 ms – i.e., significantly before the peak of the encoding component of DU_k at 500 ms. Critically, the preferred delta phase found at t* was significantly different from zero ($\varphi = -1.11 \pm 0.13$, circular t-test against zero, $p < 0.001$) – in the rising part of the delta cycle. If the effect of delta phase on decision weight w_k was generated by the transient broadband responses triggered by successive decision updates, then the maximal effect of delta phase on w_k should arguably coincide with the peak (or trough) of the delta cycle where broadband EEG signals correlate maximally with successive decision updates.

Another additional finding speaks in favour of a genuine rhythmic modulation of decision weighting: its narrow frequency selectivity (Figure S5). The spectral decomposition of transient events in broadband EEG signals typically shows a very broad frequency selectively, spanning multiple octaves. Here, by contrast, we found that the modulation of decision weighting depends selectively on the phase of EEG oscillations around 2 Hz.

Preserved neural encoding and decoding profiles at a stimulation rate of 3 Hz

To confirm that the time courses of neural encoding (Figure 2) and decision weighting (Figure 3) were not primarily driven by a fixed subharmonic of the 4 Hz stimulation frequency, we obtained additional EEG data from another group of seventeen participants who performed the same task at a different stimulation rate of 3 Hz (see Supplemental Experimental Procedures).

First, as in Figure S2, we entered previous, current and next decision updates as simultaneous parametric regressors of single-trial EEG signals and obtained three identical, overlapping time profiles, peaking positively at 550 ms after the corresponding element and shifted by 333 ms as predicted by the 3 Hz stimulation frequency (Figure S6). This first finding confirms that the neural encoding of element k after the onset of element k+1 was not contaminated in any way by the overlapping neural encoding of element k+1. Then, as in Figure S3, we estimated simultaneously the decoding time courses of successive decision weights assigned to previous, current and next elements and obtained, as above, three identical time profiles shifted by 333 ms (Figure S6). This second finding confirms that the neural decoding of decision weight w_k following the onset of element k+1 is not contaminated by the overlapping neural encoding of element k+1.

One last finding is strongly suggestive of a dissociation between the encoding/decoding profiles and the stimulation frequency: the preferred phase of the entrained f_0 oscillation at which the two profiles peak varies across the two stimulation frequencies. The preferred f_0 phase at the onset of each element was consistent across participants at both stimulation frequencies (Rayleigh test,

4 Hz: $r_{14} = 0.76$, $p < 0.001$, 3 Hz: $r_{16} = 0.58$, $p = 0.002$). Critically, however, the preferred f_0 phase taken at the average peak of the encoding/decoding profiles differed significantly between the two stimulation frequencies (two-sample Watson-Williams test, $F_{1,30} = 17.1$, $p < 0.001$). The absence of a fixed relationship between the exogenous f_0 oscillation and the encoding/decoding profiles further suggests that both profiles are governed by endogenous cortical dynamics rather than by a fixed subharmonic of the stimulation frequency f_0.

Motor beta-band activity shows key properties of the running decision variable

We finally conducted additional analyses to show that motor beta-band activity shows all characteristics of the running decision variable. If lateralised beta-band activity (10-30 Hz) at motor electrodes truly reflects a response preparation signal, then it should allow to *decode* the eventual choice (i.e., a left- vs. right-handed response) on every trial, and only *encode* the objective/veridical decision information preceding correct choices, not errors.

To verify these predictions, we assessed how motor beta-band activity encoded the sum of response updates (Figure 7) separately preceding correct choices and errors (Figure S7). As expected, we found that the neural encoding of response updates was significantly stronger in the last 500 ms preceding the onset of the response period t_R for correct choices than errors (paired t-test, $t_{14} = 4.4$, $p < 0.001$). Nevertheless, as would be expected from a response preparation signal, it was possible to decode choice from motor beta-band activity for both correct choices and errors in the same time window (t-test against zero, correct choices: $t_{14} = 5.2$, $p < 0.001$; errors: $t_{14} = 5.5$, $p < 0.001$). Interestingly, decoding accuracy diverged between correct choices and errors before 250 ms preceding the onset of the response period ($t_{14} = 2.5$, $p < 0.05$) – in other words, significant choice decoding (cluster-level $p < 0.05$) started more than 1 s earlier preceding correct choices (at t_R *minus* 1540 ms) than errors (at t_R *minus* 520 ms). This last finding suggests that errors were not primarily triggered by the neural encoding of inaccurate decision information in motor beta-band activity throughout the sequence, but rather by the lack of encoding of decision information until the end of the sequence.

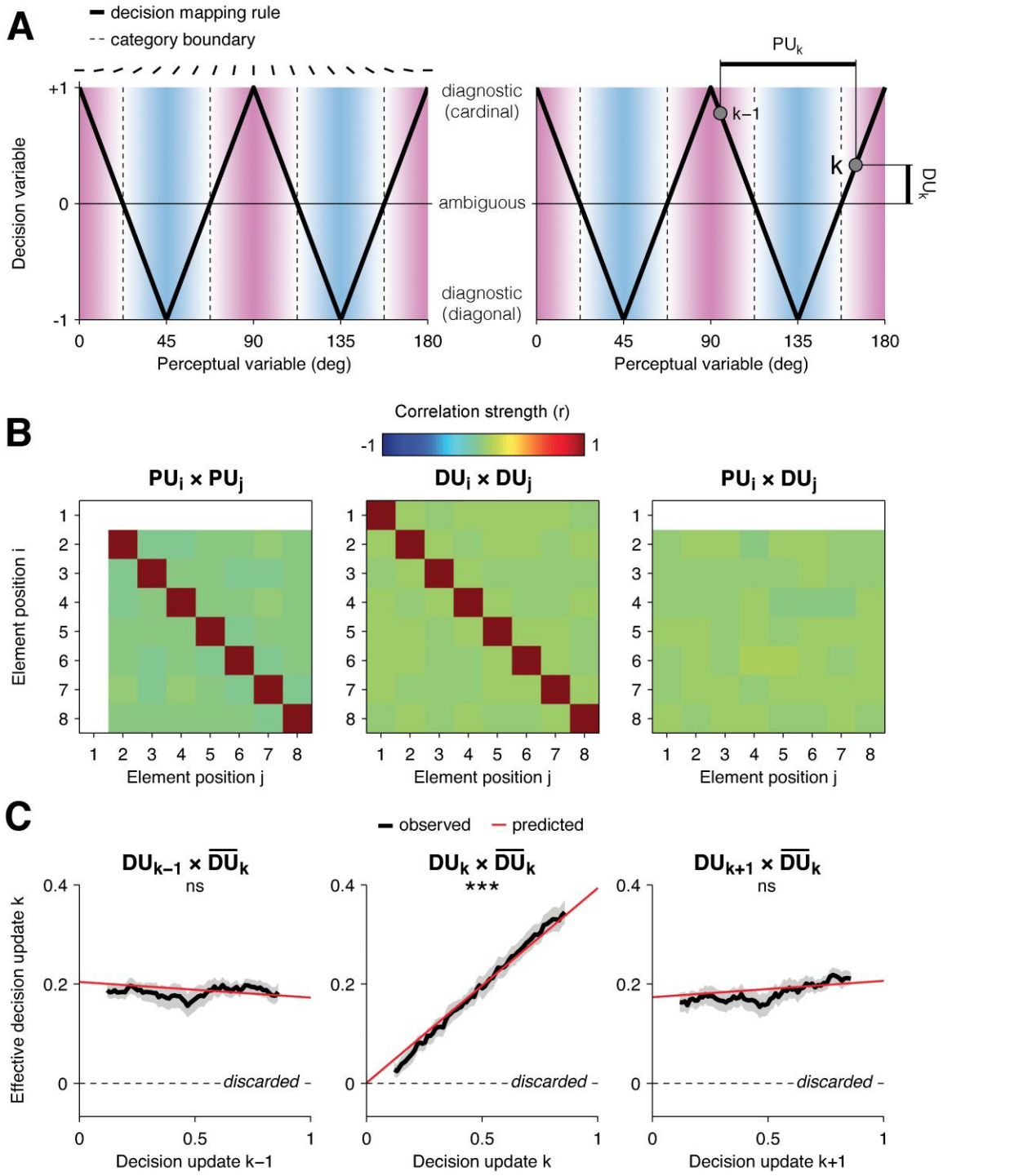

Figure S1 – Experimental design and control behavioural analysis. (**A**) Folded decision-mapping rule relating the tilt of element k (perceptual variable, x-axis) to the cardinal-diagonal decision axis (decision variable, y-axis). Left panel: the decision-mapping rule follows a w-shaped profile (thick black line) and crosses four category boundaries (dashed lines). Right panel: geometric representation of perceptual update PU_k and decision update DU_k. PU_k corresponds to the absolute difference in tilt between element k and previous element k−1, shown as the thick horizontal line. By contrast, DU_k corresponds to the absolute amount of categorical evidence provided by element k in isolation, shown as the thick vertical line. (**B**) Cross-correlation between individual perceptual and decision updates. Left panel: diagonal cross-correlation matrix among perceptual updates. Middle panel: diagonal cross-correlation matrix among decision updates. Right panel: flat cross-correlation matrix between decision (x-axis) and perceptual (y-axis) updates. (**C**) Control behavioural analysis showing orthogonal contributions of previous (left), current (middle) and next (right) decision updates to the final choice. The effective decision update assigned to element k depends solely on DU_k. Three stars indicate a significant interaction at $p < 0.001$, ns a non-significant interaction.

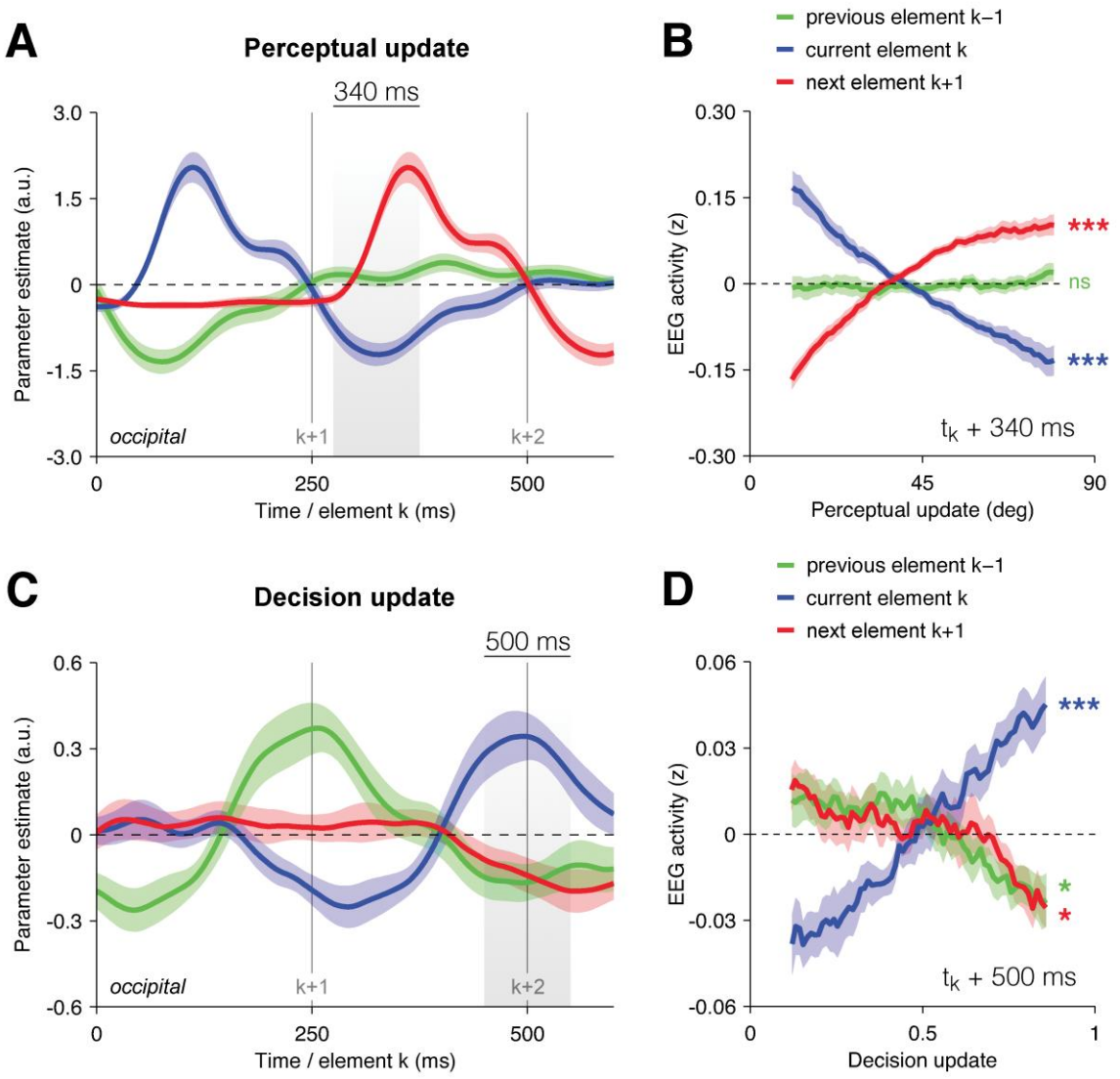

Figure S2 – Overlapping neural encoding of successive perceptual and decision updates. (**A**) Overlapping neural encoding of perceptual updates for previous (green), current (blue) and next (red) elements in EEG signals at occipital electrodes from 0 to 600 ms following element k, estimated simultaneously via a multivariate parametric regression. The shaded area highlights the negative encoding component peaking at 340 ms following element k. Shaded error bars indicate s.e.m. (**B**) Relationship between previous, current and next perceptual updates and occipital EEG activity around 340 ms following element k. Shaded error bars indicate s.e.m. Three stars indicate a significant correlation at $p < 0.001$, ns a non-significant correlation. (**C**) Overlapping neural encoding of decision updates for previous, current and next elements in EEG signals at occipital electrodes from 0 to 600 ms following element k. The shaded area highlights the positive encoding component peaking at 500 ms following element k. Same conventions as in (A). (**D**) Relationship between previous, current and next decision updates and occipital EEG activity around 500 ms following element k. One star indicates a significant correlation at $p < 0.05$. Same conventions as in (B).

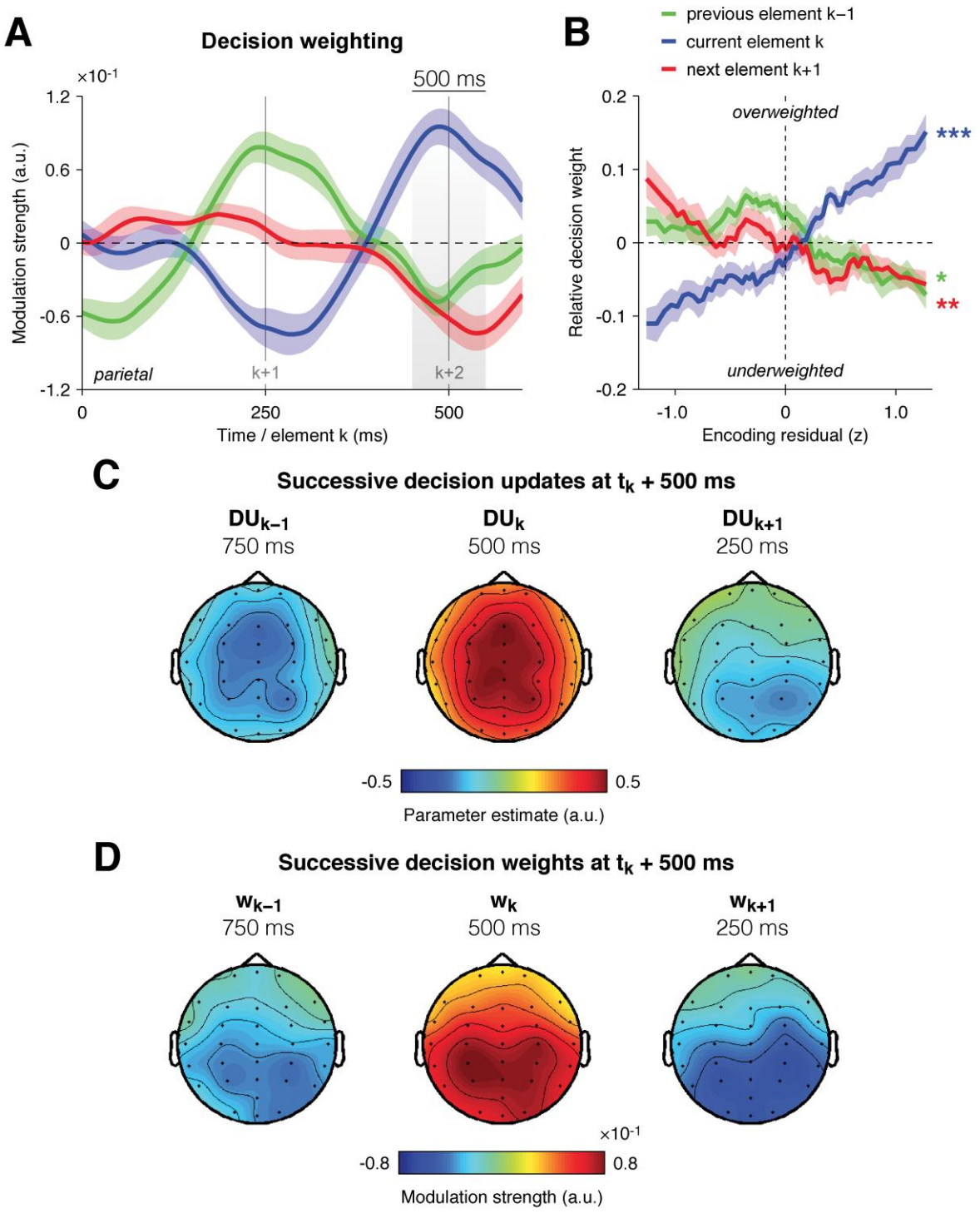

Figure S3 – Overlapping neural decoding of successive decision weights. (**A**) Overlapping neural decoding of decision weights assigned to previous (green), current (blue) and next (red) decision updates in EEG signals at parietal electrodes from 0 to 600 ms following element k, estimated simultaneously via a multivariate psycho-physiological interaction. The shaded area highlights the positive decoding component peaking at 500 ms following element k. Shaded error bars indicate s.e.m. (**B**) Relationship between encoding residuals at 500 ms following element k at parietal electrodes and successive decision weights. Encoding residuals correspond to the residuals from the parametric regression of previous, current and next decision updates against parietal EEG signals. Shaded error bars indicate s.e.m. One star indicates a significant modulation at $p < 0.05$, two stars at $p < 0.01$, three stars at $p < 0.001$. (**C**) Encoding scalp topographies of previous (left), current (middle) and next (right) decision updates at 500 ms following element k. Same conventions as in Figure 2. (**D**) Weight decoding scalp topographies of previous (left), current (middle) and next (right) decision weights at 500 ms following element k. Same conventions as in Figure 3.

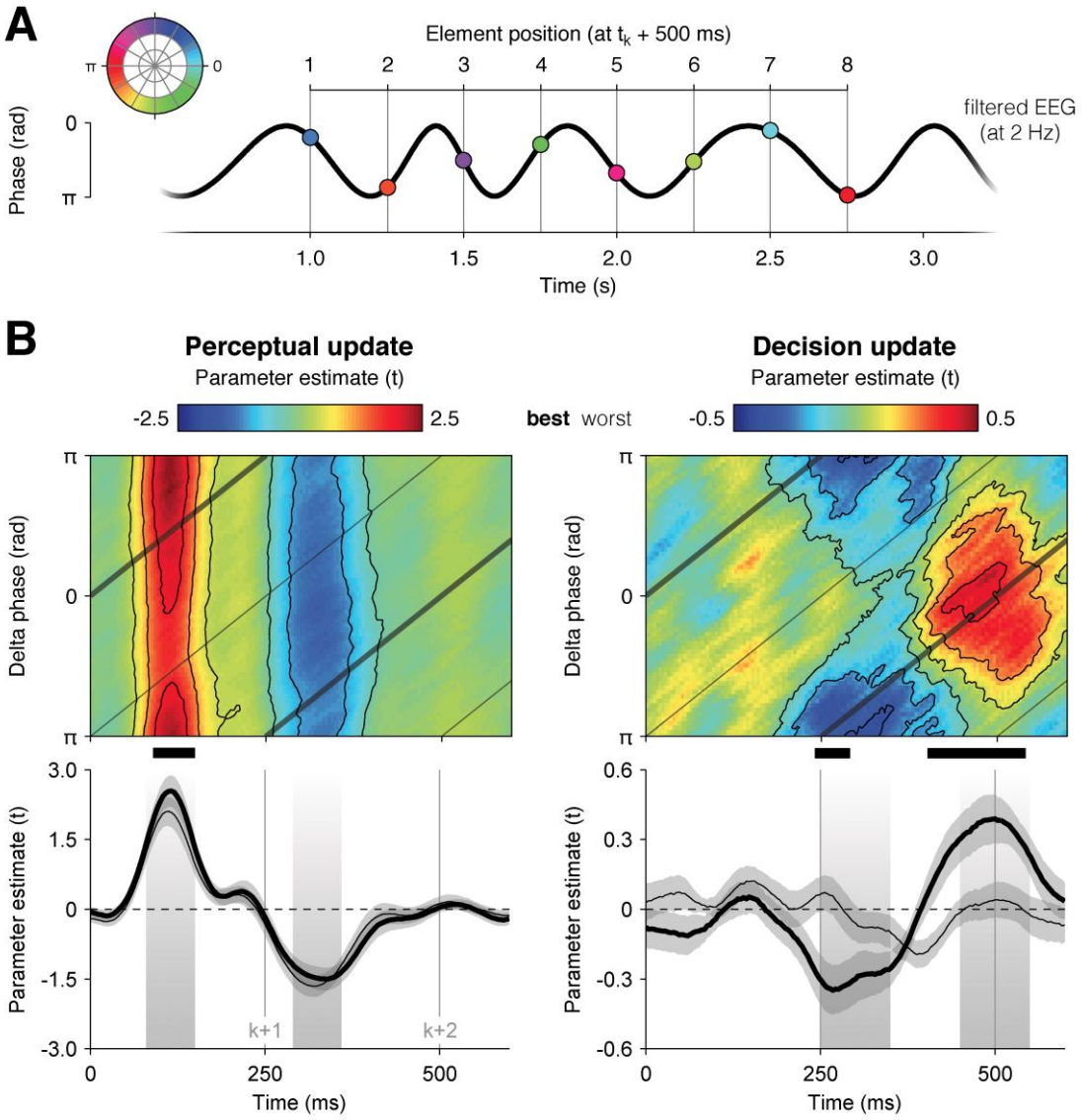

Figure S4 – Oscillatory properties of slow fluctuations in neural encoding. (**A**) Estimation of phase-dependent modulation of neural encoding or decision weighting. Trial example of the ongoing phase of parietal EEG oscillations at 2 Hz, estimated using a time-dependent wavelet transform. Coloured dots indicate EEG phase at 500 ms following the onset of each element. EEG phase is used, across trials, as a parametric modulator of the relationship between perceptual/decision updates and broadband EEG activity (neural encoding), or between decision updates and the eventual choice (weight decoding). (**B**) Oscillatory modulation of the neural encoding of perceptual (left) and decision (right) updates. Upper panels: relationship between parietal delta phase, estimated as in (A), and the neural encoding of perceptual update PU_k (left) and decision update DU_k (right), from 0 to 600 ms following element k. The predicted best (resp., worst) phase with respect to the decision weight w_k is shown as a thick (resp., thin) black line. Thick horizontal lines indicate time windows of significant phase-dependent modulations of neural encoding at $p < 0.05$ (two-tailed). Lower panels: encoding time courses of perceptual update PU_k (left) and decision update DU_k (right), following the predicted best (thick) and worst (thin) delta phase with respect to the decision weight w_k. Shaded areas highlight positive and negative encoding components. Shaded error bars indicate s.e.m.

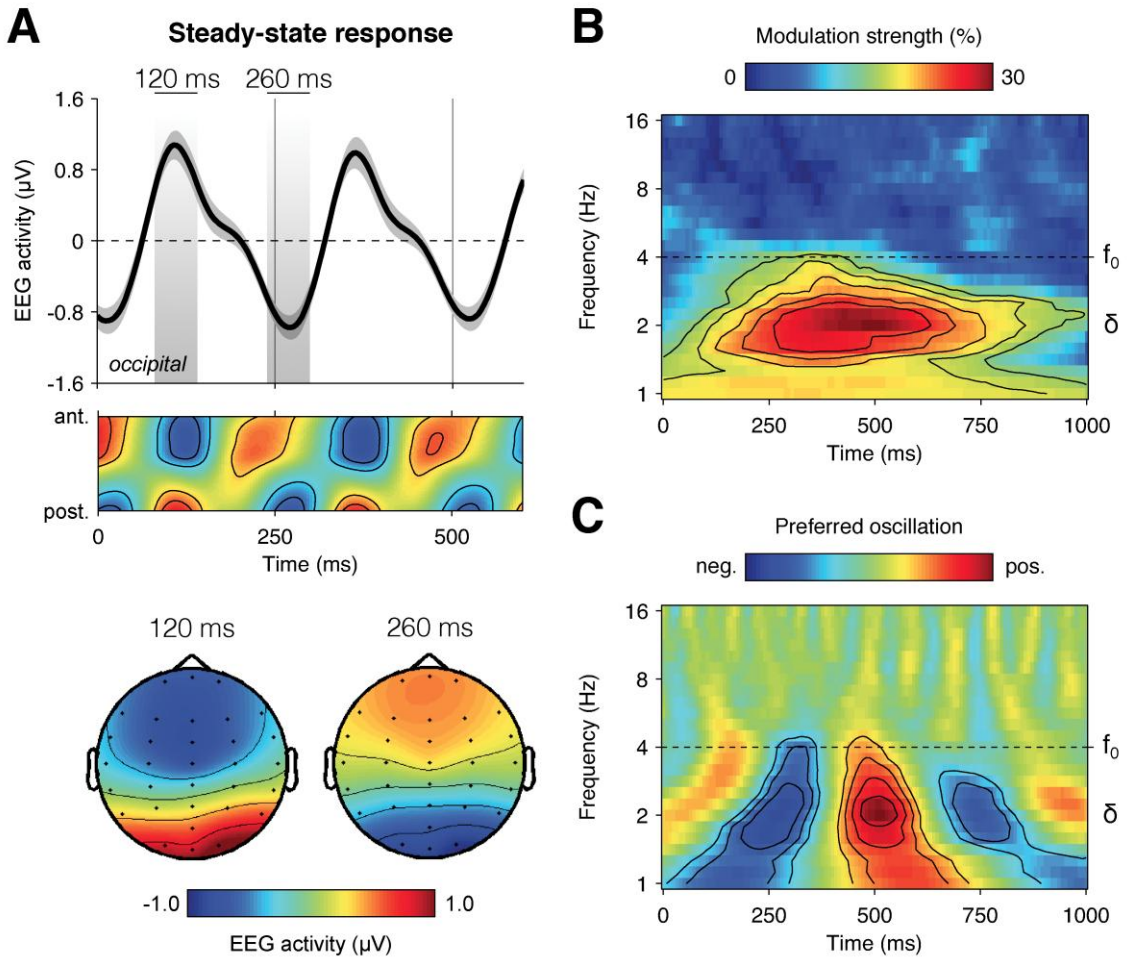

Figure S5 – Oscillatory properties of slow fluctuations in decision weighting. (**A**) Steady-state broadband response (1-16 Hz). Upper panel: steady-state response at occipital electrodes (above), and following the spatial antero-posterior gradient (below), showing a periodic time course at stimulation frequency f_0 = 4 Hz. Shaded areas highlight positive and negative peaks respectively at 120 ms and 260 ms. Lower panel: steady-state scalp topographies at 120 ms (left) and 260 ms (right). (**B**) Time-frequency profile of the phase modulation of the decision weight w_k assigned to element k between 0 and 1000 ms following element k, and between 1 and 16 Hz. The phase modulation shows a narrow spectral specificity around 2 Hz, suggestive of a genuine rhythmic process and not of a single-sided transient in EEG activity. The dashed line indicates the stimulation frequency f_0. (**C**) Time-frequency representation of the preferred oscillation with respect to the decision weight assigned to element k. Same conventions as in (B).

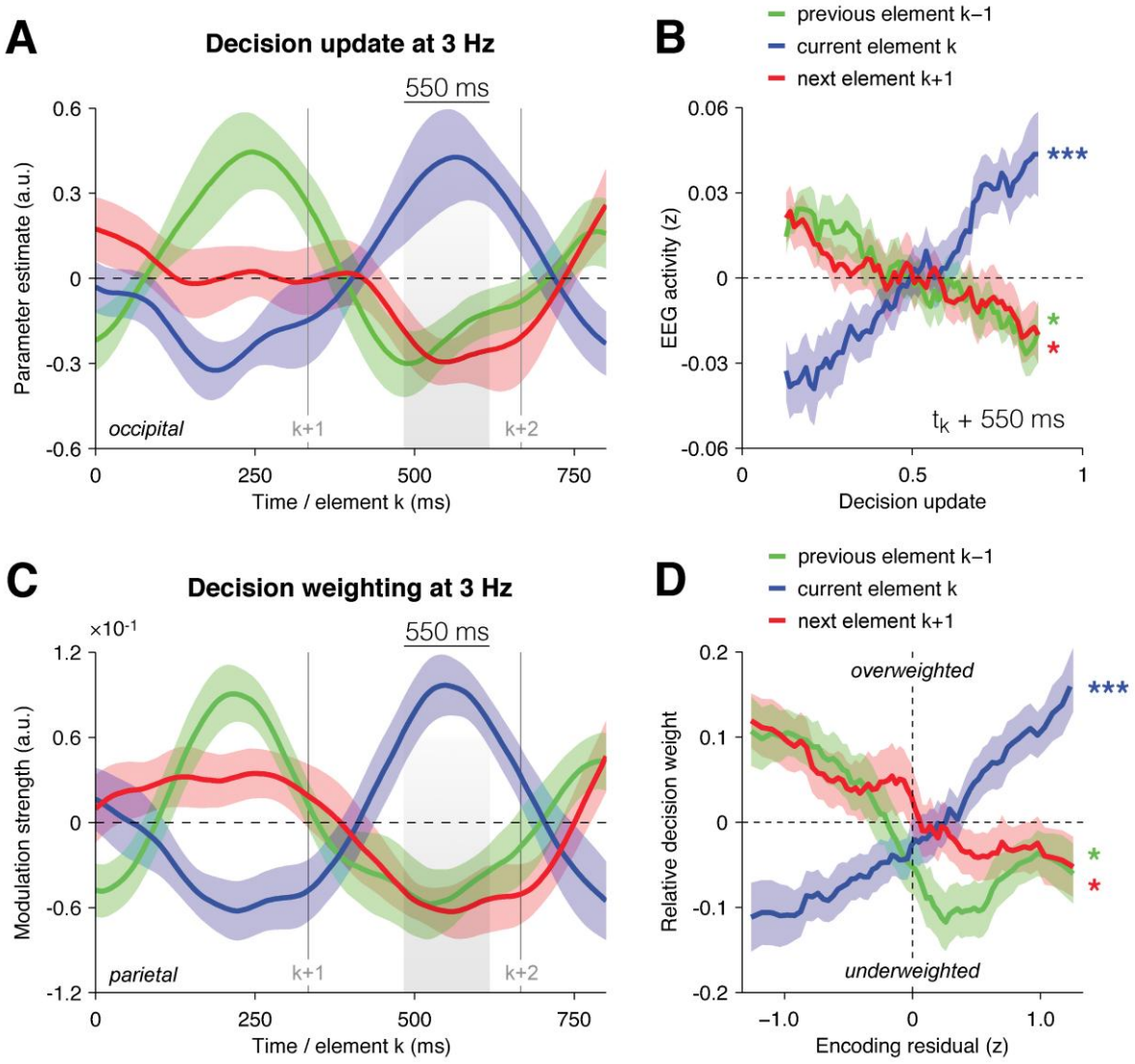

Figure S6 – Preserved neural encoding and decoding profiles at a stimulation rate of 3 Hz. (**A**) Overlapping neural encoding of decision updates for previous (green), current (blue) and next (red) elements in EEG signals at occipital electrodes from 0 to 800 ms following element k, estimated simultaneously via a multivariate parametric regression. The shaded area highlights the positive encoding component peaking at 550 ms following element k. Same conventions as in Figure S2. (**B**) Relationship between previous, current and next decision updates and occipital EEG activity around 550 ms following element k. Same conventions as in Figure S2. (**C**) Overlapping neural decoding of decision weights assigned to previous, current and next decision updates in EEG signals at parietal electrodes from 0 to 800 ms following element k, estimated simultaneously via a multivariate psycho-physiological interaction. The shaded area highlights the positive decoding component peaking at 550 ms following element k. Same conventions as in Figure S3. (**D**) Relationship between encoding residuals at 550 ms following element k at parietal electrodes and successive decision weights. Same conventions as in Figure S3.

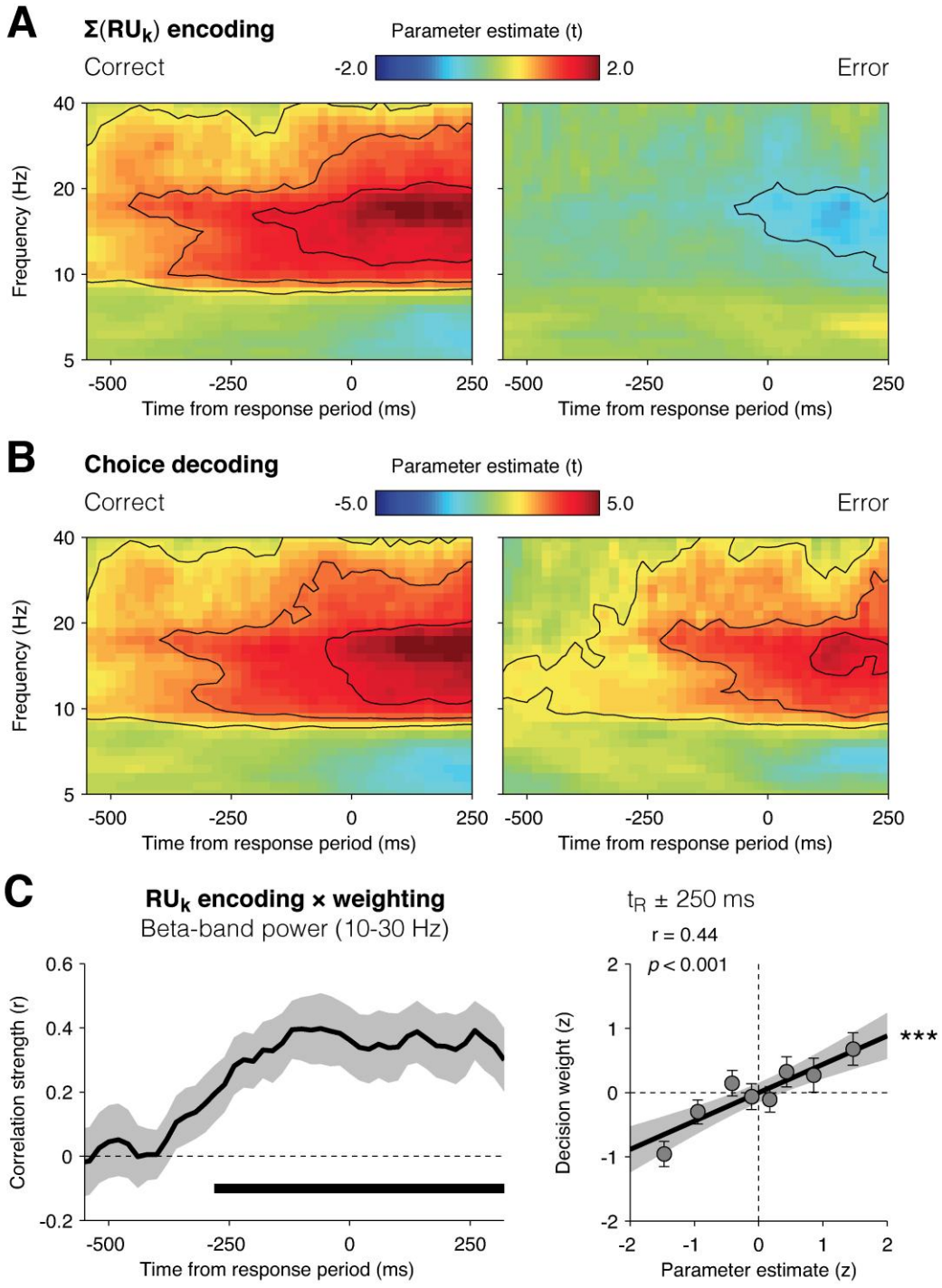

Figure S7 – Motor beta-band activity shows key properties of the running decision variable. (**A**) The neural encoding of the sum of response updates in motor beta-band activity (10-30 Hz) distinguishes correct choices (left) from errors (right) before the onset of the response period. Same conventions as in Figure 7. (**B**) By contrast, decoding choice from motor beta-band activity shows the same profile preceding correct choices (left) and errors (right). Same conventions as in Figure 7. (**C**) Single-subject, between-element correlation between the neural encoding profile of response updates in motor beta-band activity and the decision weighting profile. Left panel: neural encoding and decision weighting profiles correlate significantly from -280 ms preceding the onset of the response period. The shaded error bar indicates s.e.m. The thick horizontal line indicates significance ($p < 0.05$, two-tailed). Right panel: correlation profile at the onset of the response period t_R ±250 ms. Each dot corresponds to one element, sorted by their encoding parameter estimate. Error bars indicate s.e.m. The thick black line shows the best-fitting regression line. The shaded error bar indicates the 95 % confidence interval for the regression line. Three stars indicate a significant correlation at $p < 0.001$.

Supplemental Experimental Procedures

Here we provide a detailed comparison between our novel multi-sample categorisation task and previous decision-making studies. We also describe the procedures used for the acquisition of additional EEG data at a stimulation rate of 3 Hz (instead of 4 Hz for the original dataset).

Task design

Our multi-sample categorisation task differs in at least three main aspects from the dynamic random-dot motion stimuli most commonly used in perceptual decision-making studies (e.g., Roitman and Shadlen, 2002; Gold and Shadlen, 2003).

1. We delivered sensory evidence in eight discrete pulses instead of continuously as it is classically the case when using random-dot motion stimuli. We used this discretisation of evidence delivery in order to recover the neural processing of momentary evidence (i.e., perceptual/decision updates) in EEG signals. We reasoned that since transients in sensory stimulation were commonly used in EEG studies as a temporal reference to estimate the dynamics of visual responses (i.e., event-related potentials), delivering sensory evidence in discrete pulses would allow us to estimate the dynamics of momentary evidence processing. Recent decision-making studies have used this discretisation of evidence delivery to investigate multi-sample integration in non-human primates (Yang and Shadlen, 2007) and humans (de Lange et al., 2010; de Lange et al., 2011).

2. We delivered sensory evidence in noiseless, supraliminal (i.e., high-contrast) pulses. This feature contrasts sharply with classical random-dot motion stimuli where sensory evidence is weak and corrupted by strong external noise (i.e., at low motion coherence). This means that, while subjects cannot determine the main direction of motion from brief presentations of random-dot motion stimuli (e.g., Kiani et al., 2008), our participants could easily categorise each element in isolation as being cardinal or diagonal. Therefore, the difficulty of our multi-sample categorisation task did not arise from within-sample variability (i.e., external noise), but from a large between-sample variability on the cardinal-diagonal decision axis. In other words, cardinal elements could be followed by diagonal ones (Figure 1), such that the integration of sensory evidence across multiple samples was required – even from an optimal sensory observer – in order to perform the task accurately. By contrast, random-dot motion stimuli classically have a constant amount of coherently moving dots, such that integrating sensory evidence across time only serves to average out external noise due to suboptimal sensory processing (Mazurek et al., 2003). Here we went further by fully decorrelating successive decision updates across trials in order to perform regression-based analyses at the individual update level. This kind of analysis is precluded when using random-dot motion stimuli, because the amount of momentary evidence remains constant over the course of a single trial. Hence, only small fluctuations in external noise afford any within-trial leverage on brain activity or behaviour (Kiani et al., 2008). The large between-sample variability we used additionally ensures that the bottleneck on task performance is not set at the level of extracting low amounts of evidence from noisy sensory samples, but rather at the level of integrating successive samples with variable amounts of evidence.

3. We used a categorisation task (cardinal vs. diagonal) associated with a folded (rather than linear) decision-mapping rule (Figure S1). This seemingly minor feature of our task required participants to perform multi-sample integration in category (i.e., cardinal-diagonal) space, not in per-

ceptual (i.e., orientation) space. This feature contrasts sharply with tilt discrimination tasks for which integrating in perceptual or decision space is usually equivalent. Accordingly, an ideal (noise-free) observer performing multi-sample integration in perceptual space was found to be much worse – in terms of sensitivity d' – at predicting participants' choice behaviour than an ideal observer performing integration in category space (perceptual space: 0.39 ± 0.04, category space: 1.48 ± 0.11, paired t-test, $t_{14} = 10.2$, $p < 0.001$). The presence of a slow serial central bottleneck on evidence accumulation might be at least partially dependent on the required segregation between sensory and central stages of momentary evidence processing.

Additional dataset at 3 Hz stimulation rate

Additional EEG data was obtained at a different stimulation rate of 3 Hz from seventeen students recruited from the University of Oxford. No subject was previously recruited in the original study. All subjects had normal or corrected-to-normal vision, and reported no history of neurologic or psychiatric disorders. They provided written consent before the experiment and received £30 in compensation for their participation. The experiment followed local ethics guidelines.

Participants were faced with two streams of oriented Gabor patterns presented synchronously at 4 degrees of visual angle on the left and right of the fixation point at a stimulation rate of 3 Hz (instead of 4 Hz in the original study). In a subset of trials, participants were attending to one and ignoring the other stream according to a fully predictive cue, corresponding to a colour change in the fixation point occurring 1333 ms before the onset of the first element. All other aspects of the task were identical to the original study: following each stream, participants reported whether, on average, the tilt of the eight elements in the attended stream fell closer to the cardinal or diagonal axes by pressing either of two response buttons with the left or right index finger (DirectIN high-speed button box, Empirisoft, New York, NY), using a cardinal/diagonal response mapping fully counter-balanced across participants.

As in the original study, each participant undertook a short practice session prior to the experiment, followed by a titration session during which his or her psychophysical threshold was estimated using the same adaptive staircase procedure. This threshold estimate was then used to determine the spread of the probability distribution function used to generate the successive decision updates, resulting in a categorisation sensitivity d' of 1.48 ± 0.05. This sensitivity did not differ significantly from the categorisation sensitivity observed when pooling across easy/difficult trials in the original study (1.48 ± 0.11, two-sample t-test, $t_{30} = 0.1$, $p > 0.5$). The experiment consisted of 400 trials, divided into 8 sessions of 50 trials. The experimental condition of interest described above consisted of 200 trials.

A Neuroscan system with NuAmps digital amplifiers was used to record EEG signals from 35 Ag/AgCl electrodes, located at FP1, FP2, F7, F3, Fz, F4, F8, FT7, FC3, FCz, FC4, FT8, T7, C3, Cz, C4, T8, TP7, CP3, CPz, CP4, TP8, P7, P3, Pz, P4, P8, PO7, PO3, POz, PO4, PO8, O1, Oz, O2, plus four additional electrodes used in a bipolar montage as horizontal and vertical electro-oculograms (EOG), and two electrodes located at the mastoids used as reference. All electrode impedances were kept below 5 kΩ. EEG signals were recorded at a sampling rate of 1000 Hz and high-pass filtered online at 0.1 Hz. We applied the same EEG pre-processing pipeline as for the original study, resulting in an average of 185 ± 5 trials per participant in the experimental condition of interest described above.

Supplemental References

de Lange, F.P., Jensen, O., and Dehaene, S. (2010). Accumulation of evidence during sequential decision making: the importance of top-down factors. J. Neurosci. *30*, 731-738.

de Lange, F.P., van Gaal, S., Lamme, V.A.F., and Dehaene, S. (2011). How awareness changes the relative weights of evidence during human decision-making. PLoS Biology *9*, e1001203.

Gold, J.I., and Shadlen, M.N. (2003). The influence of behavioral context on the representation of a perceptual decision in developing oculomotor commands. J. Neurosci. *23*, 632-651.

Kiani, R., Hanks, T.D., and Shadlen, M.N. (2008). Bounded integration in parietal cortex underlies decisions even when viewing duration is dictated by the environment. J. Neurosci. *28*, 3017-3029.

Mazurek, M.E., Roitman, J.D., Ditterich, J., and Shadlen, M.N. (2003). A role for neural integrators in perceptual decision making. Cereb. Cortex *13*, 1257-1269.

Roitman, J.D., and Shadlen, M.N. (2002). Response of neurons in the lateral intraparietal area during a combined visual discrimination reaction time task. J. Neurosci. *22*, 9475-9489.

Yang, T., and Shadlen, M.N. (2007). Probabilistic reasoning by neurons. Nature *447*, 1075-1080.